PCCP

PAPER

View Article Online
View Journal | View Issue

Cite this: *Phys. Chem. Chem. Phys.*, 2015, **17**, 24349

Exploring the core level shift origin of sulfur and thiolates on Pd(111) surfaces

Roberto Carlos Salvarezza[a] and Pilar Carro*[b]

Received 16th July 2015,
Accepted 3rd August 2015

DOI: 10.1039/c5cp04180e

www.rsc.org/pccp

Thiol molecules on planar metal surfaces are widely used for building sensing and electronic devices and also as capping agents to protect and to control the size and shape of nanoparticles. In the case of Pd the thiol molecules exhibit a complex behavior because C–S bond scission is possible, resulting in a significant amount of co-adsorbed S. Therefore identification of these species on Pd is a key point for many applications, a task that is usually achieved by XPS. Here we show, from DFT calculations, that the core level shift (CLS) of the S 2p binding energy (BE) of thiol and sulfur on different thiol–Pd(111) surface models strongly depends on the adsorbed or subsurface state of sulfur atoms. Our results reflect the complexity of S 2p BE behavior and contribute to understanding and reanalyzing the experimental data of thiolated Pd surfaces.

Introduction

Palladium is a platinum group metal with many applications in fields such as hydrogen storage,[1] sensing,[2] electronics,[3] scavengers[4,5] and catalysis.[6] On the other hand, thiol molecules on planar metal surfaces are widely used for building sensing and electronic devices and also as capping agents to synthesize metal nanoparticles with exact control of size and shape.[7] Thus, thiolate-protected Pd nanoparticles have been studied for their use as hydrogen sensors due to the ability of Pd to absorb large amounts of hydrogen,[8,9] as well as for their magnetic properties.[10] Concerning the catalysis field thiolate-covered Pd catalysts have shown interesting properties such as protection against deactivation, enhanced formic acid oxidation, selectivity improvement for the synthesis of 1-epoxybutane from 1-epoxy 3-butene,[11] and catalyst activity for the formation of carbon nanotubes.[12] The catalytic activity of thiolate-covered Pd is surprising since S-containing species usually act as poisons to the Pd surface.[13] In this context it has been recently demonstrated that subsurface O species are able to increase the catalytic activity of Pd for CO oxidation under ambient conditions.[14] Therefore, elucidation of the chemistry of thiolates (RS) on Pd(111) and Pd nanoparticles (PdNPs) is a key point for understanding the interesting surface properties of these systems.

[a] *Instituto de Investigaciones Fisicoquímicas Teóricas y Aplicadas (INIFTA), Facultad de Ciencias Exactas, Universidad Nacional de La Plata – CONICET, Sucursal 4 Casilla de Correo 16, (1900) La Plata, Argentina*

[b] *Área de Química Física, Departamento de Química, Facultad de Ciencias, Universidad de La Laguna, Instituto de Materiales y Nanotecnología, Avda. Francisco Sánchez, s/n 38071-La Laguna, Tenerife, Spain. E-mail: pcarro@ull.es; Tel: +34 922 318031*

However, this issue has become challenging since it results from the interaction between a very reactive metallic surface and a strong S-containing adsorbate.[7,15] This interaction can involve different reaction pathways and surface structures depending on reaction time, temperature, thiol chemical potential, substrate defects and PdNP size.

Today it is accepted that upon thiol adsorption the reactive Pd surface induces the C–S bond cleavage of RS adsorbates.[15,16] The resulting S atoms partially passivate the Pd surface allowing further adsorption of intact RS species. Therefore, the total amount of sulfur (S + RS) on the Pd surface after thiol adsorption largely could exceed that found for thiol SAMs on coinage metals where the C–S bond cleavage is an exception.[7]

The estimation of the total content of sulfur and the relative amount of S and RS species on the metal surfaces is usually performed on the basis of X-ray photoelectron spectroscopy (XPS).[17,18] XPS data for thiol adlayers on Pd(111) and PdNPs have revealed a total sulfur coverage as large as $\theta = 0.8$.[16] On the other hand, determination of the relative amount of S and RS species on the Pd surface is a more difficult task that requires a careful deconvolution of the S 2p spectrum, and also some assumptions to assign the components.[15,16,19] In fact, the peak S 2p of XPS spectra of thiol on Pd surfaces is usually decomposed into at least two main doublets (S $2p_{3/2}$, S $2p_{1/2}$) with binding energies (BE) for the S $2p_{3/2}$ component at $\approx$162.1 eV and $\approx$162.9 eV. Earlier reports[15,16] have assigned the lower BE ($\approx$162.1 eV) to adsorbed S and the higher BE ($\approx$162.9 eV) to RS, in analogy with that found for these species on Au(111) and Ag(111) surfaces, and also from the fact that adsorbed S on Pd (111) and (100) faces exhibits S $2p_{3/2}$ BE at $\approx$162 eV.[20] On this basis, different surface structures have been proposed for the complex thiolate–S interface[15,21] starting with the $(\sqrt{3} \times \sqrt{3})$

$R30^\circ$ S ($\sqrt{3}$ S) and ($\sqrt{7} \times \sqrt{7}$) $R19^\circ$ S ($\sqrt{7}$ S) lattices, which are consistent with the estimated adsorbed S coverage and have also been observed by scanning tunneling microscopy on Pd(111),[22] and then including RS species to reach the total S content. These mixed surface structures have been modeled as ($2\sqrt{3} \times \sqrt{3}$) $R30^\circ$ S + RS and ($\sqrt{7} \times \sqrt{7}$) $R19^\circ$ S + RS, hereafter denoted as $2\sqrt{3}$ S + RS and $\sqrt{7}$ S + RS, respectively, since both models involve S, RS and total S coverage close to that derived from XPS measurements.

However, more recently, it has been suggested that the behavior of the S 2p components follows the opposite trend, *i.e.* the higher BE component corresponds to S species while the lower BE corresponds to adsorbed RS moieties.[23] Therefore, the knowledge of the S 2p core level shift (CLS) for the different species present in thiol self-assembled monolayers (SAMs) on Pd surfaces becomes crucial in order to correctly estimate their surface coverage and model the surface structures on Pd.

In this work we calculate the S 2p and Pd 3d CLS for different models of S, RS and S + RS on Pd(111)[21] from Density Functional Theory (DFT). In fact, DFT calculations are often used to interpret experimental shifts in core level binding energies.[20,24] In general, CLS reflects different phenomena:[25] the change in the charge transfer into an atom or molecule, screening effects by the surrounding atoms, molecules or substrate and redistribution of charge due to bonding and hybridization.[26,27] We explore the S 2p and Pd 3d CLSs for surface models containing adsorbed S, subsurface S, and adsorbed RS species on Pd(111), where RS species denotes methanethiol, although similar results were obtained for butanethiol on the same substrate. Our DFT calculations reveal the complexity of the S 2p assignment in real thiolate SAMs where different types of S atoms are present.

Methodology

DFT total energy calculations were carried out using the Vienna Ab Initio Simulation Package (VASP) code.[28,29] The Perdew–Burke–Enzerhoff (PBE) generalized gradient approximation (GGA)[30] functional was employed to calculate the exchange–correlation energy. The electron–ion interaction was described by the projector-augmented wave (PAW) method.[31] The Kohn–Sham one electron valence eigenstates were expanded in terms of plane-wave basis sets with a cutoff energy of 420 eV. Optimal grids of *k*-points of $9 \times 9 \times 1$, $5 \times 9 \times 1$ and $5 \times 5 \times 1$ have been used for the $\sqrt{3}$, $2\sqrt{3}$ and $\sqrt{7}$ surface models (Fig. 1), respectively. The Pd(111) surface was modeled by a five-layer slab. Surface relaxation is allowed in the top three Au layers of the slab as well as in the atomic coordinates of the adsorbates. In order to ensure the decoupling of the consecutive slabs, a 12 Å thick vacuum region is employed. The calculated lattice constant for bulk Pd was found to be 3.94 Å which is within 2% of the experimental value of 3.89 Å.[32]

The Bader analysis of the charge density has been calculated using the code developed by the Helkelman group.[33]

High quality DOS plots were obtained using very fine *k*-meshes of *k*-points of $13 \times 13 \times 1$, $9 \times 13 \times 1$ and $9 \times 9 \times 1$ for the $\sqrt{3}$, $2\sqrt{3}$ and $\sqrt{7}$ surface models (Fig. 4), respectively.

Core-level binding energy shifts (CLS) are the changes in the specific core electron binding energy (BE) between the selected atom and reference atom, being BE the energy required to remove this electron,

$$E_{\mathrm{CLS}} = \mathrm{BE} - \mathrm{BE}^{\mathrm{ref}} \quad (1)$$

The theoretical models for CLS calculations within the density functional theory can be classified into three groups, based on the complete screening picture, the transition state model and the initial state approximation, respectively. The first two models include initial and final state effects, though total energies of the systems are used in the complete screening scheme and energy eigenvalues in the transition state model. In this paper we have employed the transition model whose results are comparable with those obtained from complete screening calculations.

The transition state model is based on an extension to DFT made by Janak.[34] If the one-electron eigen energy, ε_i, depends linearly upon the occupation number, n_i, and assuming that the eigenvalues are aligned with the Fermi level zero, then:

$$E_{N+1} - E_N = \int_0^1 \varepsilon_i(n_i)\mathrm{d}n_i \quad (2)$$

$$E_{N+1} - E_N \approx \varepsilon_i(1/2) \quad (3)$$

with the $\varepsilon_i(1/2)$ evaluation at midpoint, known as Slater–Janak transition state, carried out under the assumption that the core-level is occupied by half an electron. Thus,

$$E_{\mathrm{CLS}}^{\mathrm{TS}} = -\varepsilon_i(1/2) + \varepsilon_i^{\mathrm{ref}}(1/2) \quad (4)$$

In order to determine the Pd 3d and S 2p CLSs within the Janak–Slater approach, half an electron 3d(Pd) or (2p) S has been excited from the core level to the valence region and

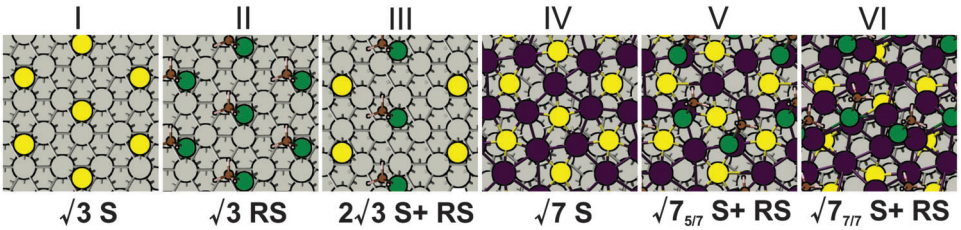

Fig. 1 Top view of the initial surface models for S and RS on the Pd(111) surface. (I) $\sqrt{3}$ S, (II) $\sqrt{3}$ RS, (III) $2\sqrt{3}$ S + RS, (IV) $\sqrt{7}$ S, (V) $\sqrt{7}_{5/7}$ S + RS, (VI) $\sqrt{7}_{7/7}$ S + RS. Gray: Pd, Magenta: reconstructed Pd, Yellow: S (S), Green: S (RS), Brown: C, Pink: H.

placed in the lowest unoccupied orbital.[20] The employed PAW pseudopotential does not include spin–orbit effects, and only the uncoupled S 2p or 3d level is provided. The Pd 3d and S 2p CLSs were referred to as bulk Pd and bulk Pd_4S, respectively.

Results and discussion

Fig. 2 contains the optimized surface structures of the models depicted in Fig. 1. While models I, II, III and IV show only slight changes with respect to the initial adsorbate positions, models V and VI exhibit strong reconstruction of the Pd top layer surface as well as changes in the adsorption site of the adsorbates. In fact, these models have initially two RS species placed on top of the $(\sqrt{7} \times \sqrt{7})$ $R19.1^\circ$ S lattice, and accordingly show an RS coverage of 2/7 (Fig. 1). Note also that the $\sqrt{7}_{5/7}$ S + RS has a Pd top layer coverage of 5/7 while the $\sqrt{7}_{7/7}$ S + RS exhibits 7/7. After geometrical optimization both surfaces exhibit a strong reconstruction with RS–Pd adatom complex formation and S and RS species located at different places from their initial positions on the Pd surface (Fig. 2).

First of all, we compare the trend in S 2p CLS and Bader charge values for models with only one type of adsorbate (Fig. 2, models I, II and IV). The S 2p CLS for S atom adsorbed in a $\sqrt{3}$ S lattice (Table 1) exhibits BE $\approx$ 0.77 eV below that the corresponding to the S atom in the $\sqrt{3}$ RS surface structure. This is the expected behavior considering that charge transfer from Pd to S atoms in the $\sqrt{3}$ S is larger than in the $\sqrt{3}$ RS surface structure, as it is shown from the Bader charge analysis. However, the opposite behaviour is found for the $\sqrt{7}$ S model (Fig. 2, IV). In this lattice the topmost layer of Pd(111) is formed by a mixed S–Pd structure with a packed arrangement of Pd pentagons with one S atom inside and two triangles including two S atoms.[35] In this case, the S atoms exhibit BE $\approx$ 0.34 eV above that found for the RS species on the $\sqrt{3}$ RS lattice, and 1.11 eV above that found for the S atoms in the $\sqrt{3}$ S lattice. Furthermore this occurs despite the fact that the S Bader charge on model IV is larger than in models I and II (Table 1). Therefore, effects other than charge transfer should be relevant to determine the complete description of S 2p CLS of this system.

Table 1 S 2p core level shift and Bader charge of S atoms in S and RS species on Pd(111) for the different surface models. Average values are indicated (S_{av}, RS_{av})

Surface model	S 2p core level shift (CLS)/eV		Bader charge/au	
Pd_4S bulk	S: 0.0		S: −0.40	
$\sqrt{3}$ S	S: −1.88		S: −0.28	
$\sqrt{3}$ RS	RS: −1.11		RS: −0.22	
$\sqrt{7}$ S	$S_1 = S_2 = S_3$: −0.77		S: −0.44	
$2\sqrt{3}$ S + RS	S: −1.87	RS: −1.30	S: −0.32	RS: −0.18
$\sqrt{7}_{5/7}$ S + RS	S_1: −1.45	RS_1: −1.67	S_1: −0.47	RS_1: −0.21
	S_2: −0.76	RS_2: −1.56	S_2: −0.39	RS_2: −0.21
	S_3: −1.09	RS_{av}: −1.62	S_3: −0.34	RS_{av}: −0.21
	S_{av}: −1.10		S_{av}: −0.40	
$\sqrt{7}_{7/7}$ S + RS	S_1: −0.47	RS_1: −1.49	S_1: −0.46	RS_1: −0.24
	S_2: −0.47	RS_2: −1.49	S_2: −0.39	RS_2: −0.22
	S_3: −1.09	RS_{av}: −1.49	S_3: −0.35	RS_{av}: −0.23
	S_{av}: −0.68		S_{av}: −0.40	

Now, we turn to the more complex $\sqrt{7}_{5/7}$ S + RS and $\sqrt{7}_{7/7}$ S + RS surface structures (Fig. 2 models V and VI).[21] For the sake of clarity we start the discussion comparing the average S 2p CLS values of these species (S_{av} and RS_{av} in Table 1) in these two

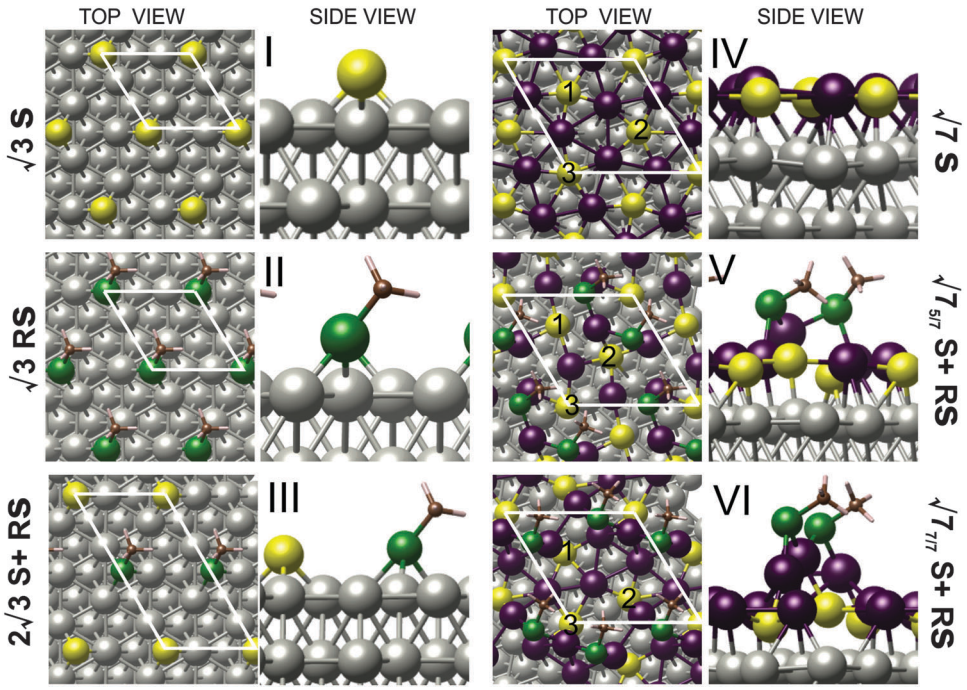

Fig. 2 Top and side view of the optimized surface models for S and RS on the Pd(111) surface. (I) $\sqrt{3}$ S, (II) $\sqrt{3}$ RS, (III) $2\sqrt{3}$ S + RS, (IV) $\sqrt{7}$ S, (V) $\sqrt{7}_{5/7}$ S + RS, (VI) $\sqrt{7}_{7/7}$ S + RS. Gray: Pd, Magenta: reconstructed Pd, Yellow: S (S), Green: S (RS), Brown: C, Pink: H. The corresponding unit cells are drawn. The sulfur atoms in Fig. (IV), (V) and (VI) have been numbered to identify their CLS and Bader charge data in Table 1.

models. For both models it can be observed that S_{av} 2p CLS of S species is 0.52 eV ($\sqrt{7}_{5/7}$ S + RS) or 0.81 eV ($\sqrt{7}_{7/7}$ S + RS) higher than the corresponding RS_{av} 2p of RS species. These figures are in good agreement with the 0.8 eV BE difference between the two S 2p components reported in the literature for thiolated Pd(111) surfaces (162.1 and 162.9 eV). However, there are several points in these mixed models (V, VI) that should be outlined. On one hand, it can be observed that the values of the Bader charge of S species are approximately constant and equal to −0.4 au, as well as equal to that Pd_4S bulk and both are very similar to those of model IV. Otherwise the S 2p CLS values for V and VI models show some differences. Thus, we note that each one of the three S atoms in the unit cell of these models exhibits quite different behavior. In fact, in the model $\sqrt{7}_{5/7}$ S + RS the BE of the S atom labeled as S_1 practically overlaps that estimated for RS moieties while S_2 and S_3 atoms have higher BE values. A similar trend is observed for the $\sqrt{7}_{7/7}$ S + RS model. From this, one can conclude that the S atoms exhibit different CLS depending on their relative positions with respect the Pd surface, depending on whether they are incorporated into the Pd substrate as subsurface atoms or they are simply adsorbed on the Pd surface. This is more clearly seen by plotting S 2p CLS *vs.* Δz, where Δz is the vertical distance between S atoms and Pd atoms of the top layer (Fig. 3a). This plot shows that adsorbed S atoms exhibit lower BE values than those corresponding to RS species, while S atoms incorporated into the metal surface as subsurface atoms show the opposite trend. This behavior is confirmed by analyzing the hypothetical model $2\sqrt{3}$ S + RS (Fig. 2, III). In this model both species, S and RS, are adsorbed on the Pd surface and the BE of the S 2p in sulfur is lower than in the RS moiety, *i.e.* the behavior observed for S atoms in the $\sqrt{3}$ S and $\sqrt{3}$ RS separated adsorption models is recovered again.

Table 2 Pd 3d core level shift and Bader charge of the Pd atom for the different surface models

Surface structures	Pd 3d core level shift (CLS)/eV	Bader charge/au
Pd bulk	0.0	0.0
Pd_4S bulk	+0.67	+0.11
$\sqrt{3}$ S	+0.86	+0.12
$\sqrt{3}$ RS	+0.42	+0.07
$2\sqrt{3}$ S + RS	+0.64	+0.09
$\sqrt{7}$ S	+1.02	+0.21
$\sqrt{7}_{5/7}$ S + RS	+0.97	+0.26
$\sqrt{7}_{7/7}$ S + RS	+0.86	+0.18

Following now with the analysis of S 2p CLS of RS species a decrease of ≈0.4/0.5 eV between model II and models V/VI is observed, *i.e.* S 2p BE values of RS species adsorbed on a sulfur passivated Pd surface (models V and VI) are lower than that on a clean and more reactive Pd surface (model II) (Fig. 3b). We attribute this decrease to the change in the Fermi levels of models V and VI with respect to model II. In fact we have obtained the differences between Fermi levels from model II to models V and VI being 0.48 and 0.51 eV, respectively.

These results indicate that the assignment to the S 2p components observed in the experimental XPS spectra is not a simple and direct task. For instance, the lower S 2p BE component could have contributions from the adsorbed (outer) S atoms and RS species (gray region in Fig. 3a). Also, it is possible that real systems formed by reaction of thiols and Pd consist of mixtures of adsorbed S and subsurface S atoms

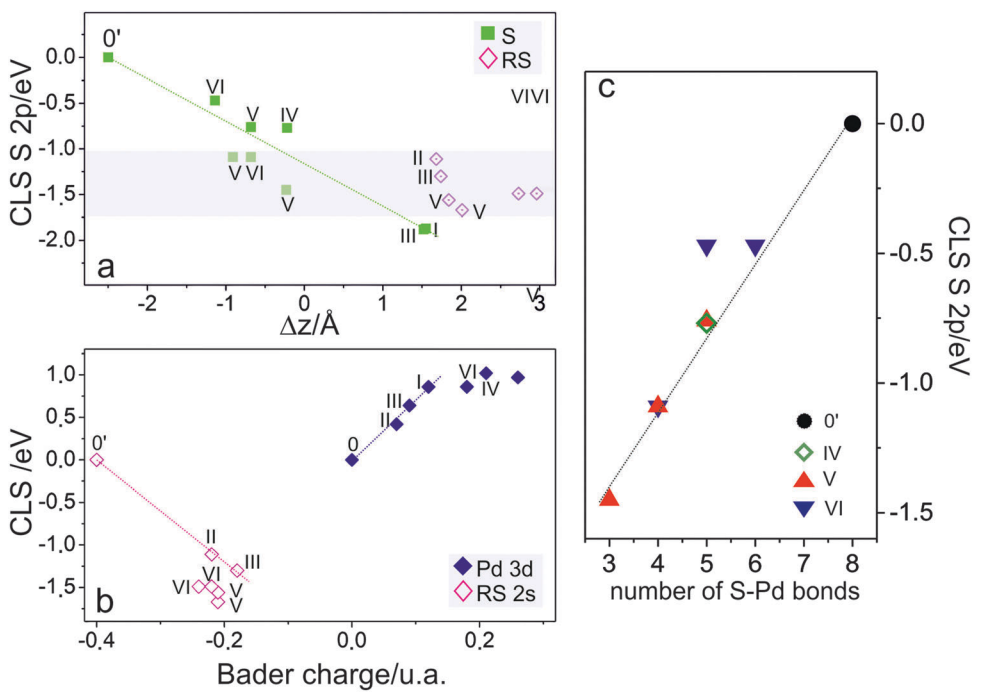

Fig. 3 (a) CLS (S 2p) *vs.* Δz for the different surface models shown in Fig. 1. (b) CLS (Pd 3d, S 2p (RS)) *vs.* Bader charge. The shaded gray region in Fig. 3a indicates the CSL values where the S and RS coexist. (c) CLS (S 2p) of subsurface sulfur species *vs.* the number of S–Pd bonds. (0) Pd (0′) Pd_4S, (I) $\sqrt{3}$ S, (II) $\sqrt{3}$ RS, (III) $2\sqrt{3}$ S + RS, (IV) $\sqrt{7}$ S, (V) $\sqrt{7}_{5/7}$ S + RS, (VI) $\sqrt{7}_{7/7}$ S + RS.

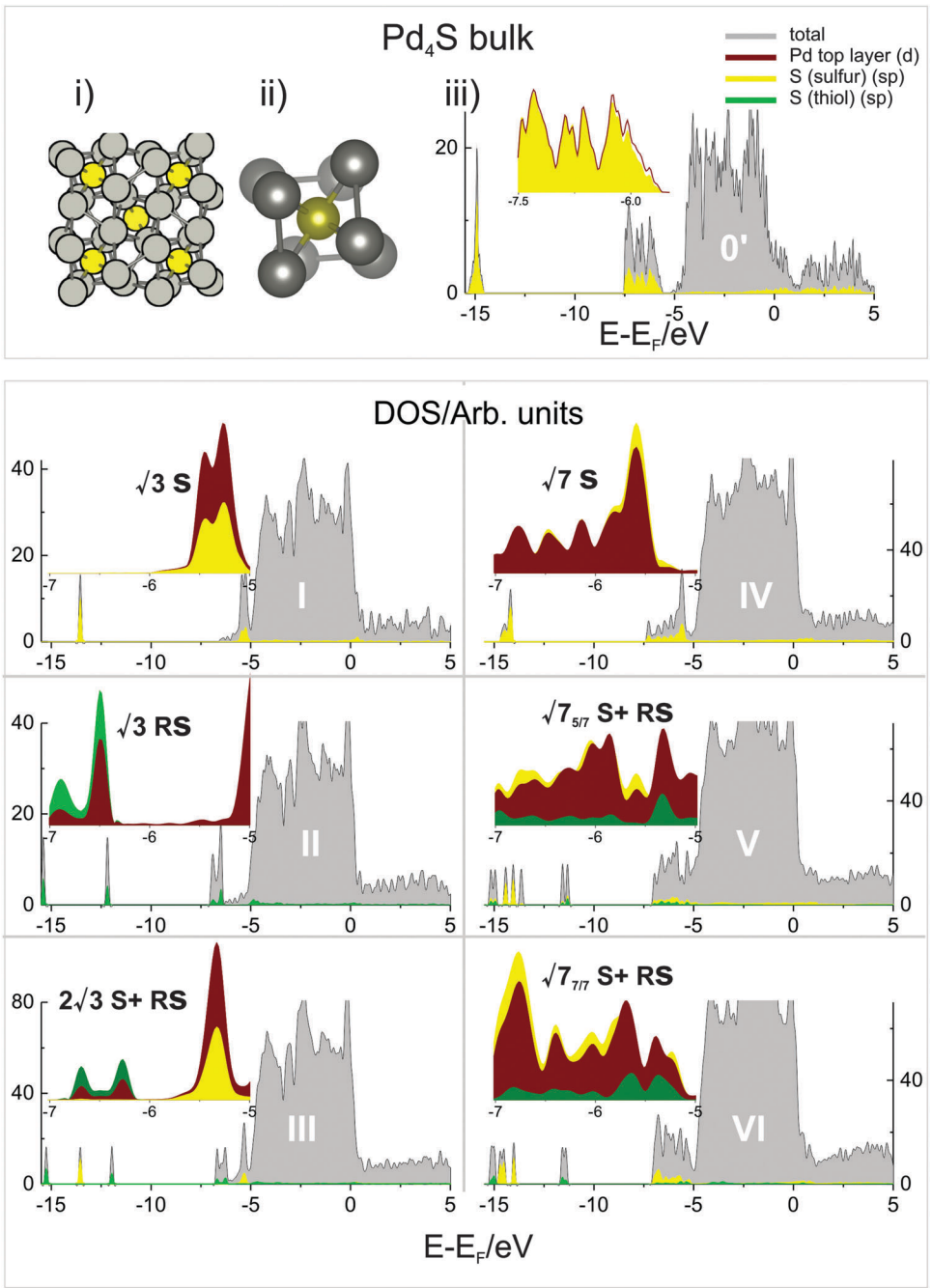

Fig. 4 Top panel: (i) optimized structure of Pd_4S bulk (reference state for S 2p CLS values). (ii) Zoom showing height Pd–S bonds of 8. (iii) Density of states (DOS) total (grey) and projected on S sp states (yellow) and Pd d states (brown). Bottom panel DOS for the optimized models projected on S sp states (S): yellow, S sp states (RS): green, top layer Pd d states: brown and total DOS: grey. The insets show PDOS in the region −7/−5 eV.

depending on the reaction time and the number of defects present on the substrate surface. In fact, adsorbed S on Pd(111) from sulfide containing solutions does not exhibit a simple S 2p spectrum as expected for equivalent S atoms in the $\sqrt{3}$ or $\sqrt{7}$ S lattices (Fig. 2, Table 1) but a more complex spectra with components between 161.6/161.7 and 162.4/162.7 eV.[16,23] Only after careful heating of the sample, the $\sqrt{7}$ S lattice is observed with S 2p component at 162.5 eV.[23] It means that the non-heated Pd surface consists of a mixed layer of different S species.

We have also analyzed the Pd 3d CLS for all the models depicted in Fig. 2 (Table 2). In the case of models containing on-surface adsorbed S atoms (I, II and III) the Pd 3d CLS values fairly correlate with the Bader charge indicating that the BEs shift positively following the magnitude of the charge transfer from the Pd atoms to the S atoms. In contrast the CLSs values remain nearly independent of the Bader charge for models containing subsurface S atoms (IV, V, and VI) (Fig. 3b). This suggests that other effects such as screening by surrounding S

atoms should be involved. Note that the experimental 3d CLS measured for the Pd surface after reaction with S and thiolate species is in the 0.2–0.65 eV range, also suggesting the presence of different species.[16,23]

In order to best understand the different behavior of the CLSs we have plotted the projected density of states (PDOS) for sulfur and palladium atoms in the surface models depicted in Fig. 2 and compared them with Pd_4S bulk, which is the reference state for the S 2p CLS (top panel, Fig. 4). Therein is shown the optimized structure for Pd_4S bulk. The analysis of the −5 eV to −7 eV energy range (bottom panel, Fig. 4) shows clear differences between S atoms in the adsorbed state and those incorporated into the Pd surface as subsurface atoms. Also, it is worthwhile to outline the good match between the PDOS of Pd_4S and model VI in the −5 eV to −7 eV range. In the models with subsurface S ($\sqrt{7}$ S, $\sqrt{7}$ S + RS models) the 3s and 3p valence states of the S atoms are hybridized with the 3d states of Pd atoms to form better bonds with Pd neighbors, stabilizing the metal surface and approaching a ''palladium sulfide'' layer. In this case the valence electrons of S atoms redistribute the charge on the 3d more diffuse states that cannot screen the nuclear charge as effectively as 3s and 3p states, *i.e.* it is more difficult to extract the S 2p core electrons, explaining the higher BEs of these models. Thus, the variation in the local valence electron density and sp-d rehybridization upon adsorption revert the trend of charge transfer to the S atoms. Note that CLSs for adsorbed species on metal surfaces have already been assigned to hybridization effects.[36] This behavior is absent in the $\sqrt{3}$ S and $2\sqrt{3}$ S + RS species where the S atoms are in an overlayer on the Pd(111) surface. In this sense, there is an interesting correlation between S 2p CLS on models IV, V and VI, *i.e.* where the S atoms are incorporated into the Pd surface with respect to the number of metal atoms that are bonded to S (Fig. 3c). The higher number of Pd coordinated to S implies best redistribution of charge due to bonding and hybridization and therefore the higher S 2p CLS. Our results demonstrate that the presence of subsurface S can induce remarkable changes in the electronic properties of Pd. In fact, it has been recently reported that subsurface O induces the electronic decoupling of the few Pd layers with the O atoms from the rest of the bulk metallic Pd, thus dramatically enhancing the catalytic activity for CO oxidation at room temperature.[14] The presence of subsurface S atoms has been also predicted by molecular dynamic calculations for S and RS covered Pd nanoparticles where S atom are located at the first and second Pd layers promoting strong reconstruction of the Pd surface.[37]

Conclusions

Our results shed light on the S 2p XPS spectra of thiolated Pd(111) surfaces. We have demonstrated that the relative S 2p BE value of RS with respect to the S species, arising from the C–S bond cleavage, strongly depends on the vertical position of the S atom with respect to the topmost surface layer, above (adsorbed configuration) or below (subsurface configuration) the Pd(111) surface. Also, the components in S 2p spectra could have mixed contributions from RS species as well as adsorbed S atoms. Finally, charge transfer effects dominate the CLS of S 2p and Pd 3d for models containing adsorbed S, while hybridization and screening effects become more relevant when subsurface S atoms are present on the Pd(111) surface.

Acknowledgements

The authors acknowledge financial support from ANPCyT (PICT 2554) and CONICET (PIP 00362), both from Argentina, and CTQ2011-24784 from Spain. P. C. thankfully acknowledges the computer resources provided by Atlante, Canary Islands Supercomputing Infrastructure – Red Española de Supercomputación – and by the Computer Support Service for Research (SAII) at La Laguna University.

References

1 F. D. Manchester, A. San-Martin and J. M. Pitre, *J. Phase Equilib.*, 1994, **15**, 62–83.
2 F. Favier, E. C. Walter, M. P. Zach, T. Benter and R. M. Penner, *Science*, 2001, **293**, 2227–2231.
3 M. Antler, *Platinum Met. Rev.*, 1982, **26**, 106–117.
4 A. W. J. Smith, S. Poulston, L. Rowsell, L. A. Terry and J. A. Anderson, *Platinum Met. Rev.*, 2009, **53**, 112–122.
5 B. Mondal, R. D. Wilkes, J. M. Percy, T. Tuttle, R. J. G. Black and C. North, *Dalton Trans.*, 2014, **43**, 469–478.
6 M. Hooper, *Platinum Met. Rev.*, 2005, **49**, 77.
7 C. Vericat, M. E. Vela, G. Corthey, E. Pensa, E. Cortés, M. H. Fonticelli, F. Ibañez, G. E. Benitez, P. Carro and R. C. Salvarezza, *RSC Adv.*, 2014, **4**, 27730–27754.
8 F. J. Ibañez and F. P. Zamborini, *Langmuir*, 2006, **22**, 9789–9796.
9 F. J. Ibañez and F. P. Zamborini, *Small*, 2012, **8**, 174–202.
10 R. Litrán, B. Sampedro, T. C. Rojas, M. Multigner, J. C. Sánchez-López, P. Crespo, C. López-Cartes, M. A. García, A. Hernando and A. Fernández, *Phys. Rev. B: Condens. Matter Mater. Phys.*, 2006, **73**, 054404.
11 S. T. Marshall, M. O'Brien, B. Oetter, A. Corpuz, R. M. Richards, D. K. Schwartz and J. W. Medlin, *Nat. Mater.*, 2010, **9**, 853–858.
12 S. Lee, M. Yamada and M. Miyake, *Sci. Technol. Adv. Mater.*, 2005, **6**, 420–426.
13 B. P. S. Chauhan, J. S. Rathore and T. Bandoo, *J. Am. Chem. Soc.*, 2004, **126**, 8493–8500.
14 C. S. Gopinath, K. Roy and S. Nagarajan, *ChemCatChem*, 2015, **7**, 588–594.
15 J. Christopher Love, D. B. Wolfe, R. Haasch, M. L. Chabinyc, K. E. Paul, G. M. Whitesides and R. G. Nuzzo, *J. Am. Chem. Soc.*, 2003, **125**, 2597–2609.
16 G. Corthey, A. A. Rubert, G. A. Benitez, M. H. Fonticelli and R. C. Salvarezza, *J. Phys. Chem. C*, 2009, **113**, 6735–6742.
17 D. Spanjaard, C. Guillot, M. Desjonquères, G. Tréglia and J. Lecante, *Surf. Sci. Rep.*, 1985, **5**, 1–85.

18 S. Hüfner, *Photoelectron Spectroscopy: Principles and Applications*, Springer, Berlin, 2003.
19 G. Corthey, A. A. Rubert, A. L. Picone, G. Casillas, L. J. Giovanetti, J. M. Ramallo-López, E. Zelaya, G. A. Benitez, F. G. Requejo, M. José-Yacamán, R. C. Salvarezza and M. H. Fonticelli, *J. Phys. Chem. C*, 2012, **116**, 9830–9837.
20 K. Gotterbarm, N. Luckas, O. Höfert, M. P. A. Lorenz, R. Streber, C. Papp, F. Viñes, H. Steinrück and A. Görling, *J. Chem. Phys.*, 2012, **136**, 094702.
21 P. Carro, G. Corthey, A. A. Rubert, G. A. Benitez, M. H. Fonticelli and R. C. Salvarezza, *Langmuir*, 2010, **26**, 14655–14662.
22 J. G. Forbes, A. J. Gellman, J. C. Dunphy and M. Salmeron, *Surf. Sci.*, 1992, **279**, 68–78.
23 J. Jia, A. Bendounan, K. Chaouchi, S. Kubsky, F. Sirotti, L. Pasquali and V. A. Esaulov, *J. Phys. Chem. C*, 2014, **118**, 24983–24994.
24 M. Van Den Bossche, N. M. Martin, J. Gustafson, C. Hakanoglu, J. F. Weaver, E. Lundgren and H. Grönbeck, *J. Chem. Phys.*, 2014, **141**, 0347006.
25 P. S. Bagus, F. Illas, G. Pacchioni and F. Parmigiani, *J. Electron Spectrosc. Relat. Phenom.*, 1999, **100**, 215–236.
26 J. L. Cabellos, D. J. Mowbray, E. Goiri, A. El-Sayed, L. Floreano, D. G. De Oteyza, C. Rogero, J. E. Ortega and A. Rubio, *J. Phys. Chem. C*, 2012, **116**, 17991–18001.
27 M. Weinert and R. E. Watson, *Phys. Rev. B: Condens. Matter Mater. Phys.*, 1995, **51**, 17168–17180.
28 G. Kresse and J. Hafner, *Phys. Rev. B: Condens. Matter Mater. Phys.*, 1993, **48**, 13115–13118.
29 G. Kresse and J. Furthmüller, *Comput. Mater. Sci.*, 1996, **6**, 15–50.
30 J. P. Perdew, K. Burke and M. Ernzerhof, *Phys. Rev. Lett.*, 1996, **77**, 3865–3868.
31 P. E. Blöchl, *Phys. Rev. B: Condens. Matter Mater. Phys.*, 1994, **50**, 17953–17979.
32 C. Kittel, *Introduction to Solid State Physics*, Wiley, New York, 1986.
33 G. Henkelman, A. Arnaldsson and H. Jónsson, *Comput. Mater. Sci.*, 2006, **36**, 354–360.
34 J. F. Janak, *Phys. Rev. B: Condens. Matter Mater. Phys.*, 1978, **18**, 7165–7168.
35 W. Liu, K. A. R. Mitchell and W. Berndt, *Surf. Sci.*, 1997, **393**, L119–L125.
36 I. Hong, C. Cheng and T. Pi, *Phys. Rev. B: Condens. Matter Mater. Phys.*, 2007, **75**, 165412.
37 G. Corthey, J. A. Olmos-Asar, G. Casillas, M. M. Mariscal, S. Mejía-Rosales, J. C. Azcárate, E. Larios, M. José-Yacamán, R. C. Salvarezza and M. H. Fonticelli, *J. Phys. Chem. C*, 2014, **118**, 24641–24647.